NEUTRAL WINDS DERIVED FROM IRI PARAMETERS AND FROM THE HWM87 WIND MODEL FOR THE SUNDIAL CAMPAIGN OF SEPTEMBER, 1986.

K. L. Miller,[1] A. E. Hedin,[2] P. J. Wilkinson,[3] D. G. Torr,[4] and P. G. Richards[4]

[1]Utah State University, Logan, UT 84322; [2]Goddard Space Flight Center, Greenbelt, MD 20771; [3]IPS Radio and Space Services, Darlinghurst N.S.W., 2010, Australia, [4]University of Alabama, Huntsville, AL 35899.

ABSTRACT

Meridional neutral winds from the HWM87 empirical neutral wind model and derived from predictions of the International Reference Ionosphere are compared with neutral winds derived from ionosonde measurements of the height of the maximum ionization of the *F2*-layer. The time period considered in this study is the SUNDIAL-2 campaign, 21 September through 5 October 1986. Neutral winds along magnetic meridians have been derived from measurements by a global network of ionosondes, and compared on a global scale with winds derived from similar quantities generated by the International Reference Ionosphere and with the geomagnetically-northward component of the winds from the HWM87 model. Global wind patterns from the three sources are similar. Differences tend to be the result of local or transient phenomena that are either too rapid to be described by the order of harmonics of the empirical models, or are the result of temporal changes not reproduced by models based on average conditions. A fit of median wind speeds to 24, 12, and 8-hour waves indicates that a representation of the winds in the *F*-region that is based on periodic functions can give an accurate estimate of the global meridional wind field.

INTRODUCTION

An accurate estimate of the meridional neutral wind in the thermosphere is one of the more important prerequisites in any model of the *F2* region of the ionosphere. An inaccurate neutral wind value can change the height of the modelled *F2* peak by tens of kilometers. Unfortunately, there is a lack of global-scale neutral wind measurements, making it difficult to verify the models. Measurements have been limited to infrequent and scattered observations by Fabry-Perot interferometers, values derived from ion drift measurements by incoherent scatter radars and data from a few optical instruments and mass spectrometers on satellites. This paper discusses two models that are being developed that have the potential of providing predictions of average wind conditions in the thermosphere. An exploratory study compares the winds from these two models with meridional winds derived from ionosonde measurements.

The two methods considered here for deriving meridional neutral winds are the 1987 Horizontal Wind Model (HWM87) (Hedin *et al.*, 1988), and a derivation based on the height of the maximum ion density of the *F2*-region (*hmF2*), which uses a combination of the *hmF2* prediction from the International Reference Ionosphere (IRI) (Rawer *et al.*, 1978; Rawer and Ramanamurty, 1985) and a calculation of the dependence of *hmF2* on the neutral meridional wind by the Field Line Interhemispheric Plasma Model (FLIP) (Richards and Torr, 1985; Young *et al.*, 1980; Chandler *et al.*, 1983). Only HWM87 gives the wind speed directly. Winds from the IRI and FLIP models were derived by considering the difference between the height of the *F2* layer

as given by the IRI and the balance height, or the height of the *F2* layer if there were no neutral wind (Miller *et al.*, 1986; Miller *et al.*, 1987; Miller and Torr, 1987). Near the height of the peak electron density of the *F2* region the response of the layer to changes in the wind is approximately linear (Rishbeth, 1966; Buonsanto, *et al.*, 1989), and can be modelled by the FLIP model. Only the component of the wind parallel to the magnetic field affects the layer height. In this paper, the horizontal component of the neutral wind along a geomagnetic meridian will be referred to as the meridional wind.

WINDS FROM THE HWM87 MODEL

The HWM87 neutral wind model (Hedin *et al.*, 1988) was developed from cross-track wind measurements by the NATE mass spectrometer on the Atmospheric Explorer-E satellite (AE-E), from zonal wind data from the WATS mass spectrometer on the Dynamics Explorer-2 (DE-2) satellite, and from meridional wind data from optical measurements of the Doppler shifts of atmospheric emissions as measured by the FPI instrument of the DE-2 satellite. AE-E was in a near-equatorial orbit and DE-2 was in a polar orbit. Coefficients for the model were determined by fitting wind data to vector spherical harmonic base functions, in much the same way as was done for scaler quantities in the MSIS neutral atmosphere model (Hedin, 1987). At present, the HWM87 model includes annual and UT variations of the neutral wind at arbitrary geographic locations. Dependence of wind velocities on magnetic activity is described

by a ratio to magnetically quiet conditions based on either the 24-hour A_p index or the 3-hour a_p index. No dependence on solar flux variability is presently included in the model.

The HWM87 model provides geographically zonal and meridional components of the neutral wind in the *F* region. The other two methods for deriving neutral winds that are considered in this paper are sensitive only to the component of the wind that is parallel to a geomagnetic meridian. The corresponding component of the wind from the HWM87 model was found by projecting the wind vector onto the magnetic meridian defined by the IGRF geomagnetic field model. The declination of the geomagnetic field is less than about 20 degrees over most of the globe, but becomes especially large in the Southern Hemisphere near 90 degrees east longitude.

WINDS INFERRED USING THE IRI AND FLIP MODELS

The height of the ionization maximum in the *F2* layer (*hmF2*) is typically greater at nighttime than daytime at mid-latitudes. The change in height is primarily the result of pressure-induced neutral flow from the day side to the night side. The poleward flow in the daytime pushes the layer down the magnetic field to lower altitudes; similarly, the equatorward flow at night raises the layer.

At wind speeds that are typical in the F region, the response of the height of the ionization layer to changes in the speed of the meridional component of the neutral wind is approximately linear (Rishbeth, 1966; Buonsanto *et al.*, 1989). Miller *et al.*

(1986) took advantage of this linear relationship to develop a technique to derive the neutral wind speed from measurements of *hmF2*. According to their method, the neutral wind along the magnetic meridian is derived from a comparison of *hmF2* and the balance height, or the height where, in the absence of neutral winds, recombination and diffusion alone determine the peak of the *F2* layer would be located.

The FLIP Model (Richards and Torr, 1985; Young *et al.*, 1980; Chandler *et al.*, 1983) is used to determine both the balance height (h_o) and the ratio that expresses the linear relationship between changes in layer height and changes in neutral wind speed (α). The O^+-O collision cross-section of Banks (1966) was used in the model computation. Recent studies have suggested that the cross-section should be increased by about a factor of 1.7 (Burnside, *et al.*, 1987). If the larger value had been used in this study, the variability of the winds that are derived from *hmF2* would not be affected, but their magnitudes would be reduced significantly (Buonsanto, *et al.*, 1989).

Examples of the diurnal variation of h_o and α for conditions representative of this study are shown in Figures 1 and 2. These examples are typical of mid-latitude stations. Since the FLIP model is limited to regions of closed field lines and does not include effects of convection electric fields, high and low latitudes are not included in this study.

One of the basic parameters provided by the IRI is *hmF2*. The *hmF2* estimates are calculated from the CCIR maps of *M(3000)F2*, and include a correction for the underlying ionization that is based on the ratio of *foF2* to *foE*, (Rawer and

Ramanamurty, 1985; Dudeney, 1983). Since *hmF2*, as given by the IRI, is based on an empirical fit to data, it should represent average conditions in the ionosphere. An estimate of the meridional neutral wind derived from *hmF2* values from the IRI should therefore represent the meridional neutral wind which, under the specified conditions, would raise or lower the peak density from the balance height to the height predicted by the IRI.

Figure 3 shows the layer height at one of the ionosonde sites used in this study. The short dashes show the balance height, while the long dashes and solid lines are *hmF2* predicted by the IRI model and derived from ionosonde measurements of the critical frequencies. The ionosonde values are 15-day medians of the derived *hmF2* for the SUNDIAL-2 measurement campaign. The meridional wind is derived from the difference between *hmF2* and h_o, divided by α.

WINDS FROM IONOSONDE DATA

Meridional wind speed has been derived for the SUNDIAL-2 study using ionosonde critical frequency measurements, providing a comparison to the two empirical models discussed above. This was a moderately active period, with K_p ranging between 1 and 6 (Figure 4). *hmf2* was derived from *M(3000)F2* by the formula of Dudeney (1983), which uses *foE* and *foF2* to correct for effects of underlying ionization. Since winds derived from the ionosonde data were to be compared with calculations based on models representing average conditions, median values were found for the ionosonde

winds from all 15 days of the SUNDIAL-2 campaign.

Ionosonde data were obtained from the global ionosonde network and used together with other ionosonde data collected in the SUNDIAL-2 campaign. The network yields a broad coverage of the globe, and demonstrates one advantage of this technique, in that a near-global picture of meridional winds can be derived.

COMPARISON OF WIND RESULTS

CONTOUR MAPS

Figures 5 through 7 are global representations of the meridional neutral wind at 0 UT from the three methods described above. A contour map of meridional neutral wind speed for the middle of the SUNDIAL-2 campaign computed by the HWM87 model is presented in Figure 5. Figure 6 shows wind values derived from IRI predictions of *hmF2*. Figure 7 shows contours of meridional neutral wind speed derived from ionosonde critical-frequency measurements. The locations of ionosondes contributing to Figure 7 are marked by the symbols.

An A_p of 13 was assumed for the HWM87 winds in Figure 5. This was the median value for the fifteen days of the SUNDIAL-2 campaign. Figure 8 shows the diurnal variation of the winds predicted by the HWM87 model for Poitiers, France for equinox conditions, but using three different A_p values. The model indicates a strong dependence of the winds on magnetic activity.

Wind speeds from the IRI (Figure 6) were derived from predictions for September and for October which were interpolated to September 28, the middle of the SUNDIAL-2 campaign. Contours have not been extended to the polar region or across the magnetic equator. In its present form, this technique for deriving neutral winds is restricted to closed field lines and does not allow for the effects of convection electric fields, and so is not valid near the magnetic dip equator or at high magnetic latitudes.

Meridional wind speeds derived from ionosonde measurements (Figure 7) were gridded directly from averages of the 15 days of the SUNDIAL-2 campaign. The pattern is dependent on the distribution of data points. No attempt was made to fill in the areas lacking in ionosonde data. Much greater differences are seen between the Northern and Southern Hemispheres in Figure 7 than in the previous two figures. Many of the differences are due to the large areas of the globe where there are no ionosondes. The IRI results are also based on the ionosonde network and suffer from the same uneven coverage.

The SUNDIAL-2 campaign was at equinox, and the three contour patterns appear to be roughly symmetric about the equator. The strongest asymmetry is the distortion of the contours by the offset of the geomagnetic equator. The fact that the zero in the HWM87 model results shown in Figure 5 appears to follow the geomagnetic equator indicates that this feature is not an artifact of the technique of deriving neutral winds from ionospheric quantities, but is the result of ion drag on the motions of the

neutral atmosphere.

All three wind patterns show a north-south asymmetry in the maximum wind speed. This asymmetry is strongest at night. Local midnight is at 0 UT in the figures. The nighttime wind toward the equator is greatest over Europe in each of the figures. The daytime poleward wind appears to be strongest in the Southern Hemisphere in the HWM87 predictions of Figure 5, although this is not supported by the other two contour plots.

STATION-TO-STATION COMPARISON

The symbols in Figure 7 show the location of the ionosondes contributing to this study. There are several combinations of stations that one could consider. Data from two chains of stations are presented here to demonstrate latitudinal and longitudinal variations in the results. The stations of these two chains are designated by the open symbols in the figures.

Figure 9 shows the meridional wind speed for the series of stations at approximately constant geographic latitude across northern Europe and Asia This chain of ionosonde stations is designated by open circles in the Figure 7. The geographic location is specified on Figure 9 after the station name. These stations are all about 50 degrees north geographic latitude, and geomagnetically near L = 2.7. The data are plotted as a function of universal time. In each plot, ionosonde winds are shown by stars, winds inferred from the IRI and FLIP models by a solid line, and winds from the

HWM87 model by a dashed line. Local noon and midnight are marked by the open and shaded circles, respectively.

Immediately apparent in this figure is the good agreement between the ionosonde winds and the IRI winds. Since the wind is derived from each using the same technique, this is equivalent to the statement that the average values of *hmF2* during this period are reproduced very well by the IRI. One of the few consistent departures from this agreement is the smaller night time southward wind that is predicted by the IRI near 18 hours UT The abatement in the IRI wind appears to be fixed at a constant Universal Time, and is possibly an artifact of the harmonic series used to generate the CCIR maps for the IRI. There is also a sunrise peak in the ionosonde wind immediately after it turns northward that is not present in the IRI.

Winds from the HWM87 model are characterized by slower variation at sunrise and sunset, reflecting the harmonic base functions which are expanded to third order in the HWM87 model. The rapid changes at sunrise and sunset and other features lasting only a few hours would require an increase in the order of the harmonic functions used in the model.

Figure 10 shows winds from a meridional chain of stations through Japan and Australia designated by diamonds in the contour plots. The same comments can be made here concerning the inability of the HWM87 model to follow the rapid temporal variations. However, the amplitude of the diurnal variation is generally reproduced by all three results. The tendency of the poleward wind to remain constant during the day

that is seen in the ionosonde winds at the northern stations is also apparent in the low latitude stations. This figure also shows a significant semi-diurnal component at low latitude.

The abatement in the nighttime wind that occurs at 18 UT in Figure 9 is also apparent in Figure 10. This feature is common to all latitudes in the winds from the IRI, and, as was stated, may be an artifact of the harmonics used in the model. However, it is matched by the data in the Southern Hemisphere, beginning at Vanimo and continuing south through much of Australia. The fact that this feature is consistently present through 15 days indicates that it is likely to be tidal in origin.

FOURIER COMPONENTS IN THE WIND DATA

An estimation of the tidal components in the data was made to see if this nighttime abatement might be the result of 12- and 8-hour tides, as it is at Arecibo (Burnside, *et al.*, 1983; Crary and Forbes, 1986). This was done by fitting the median winds derived from ionosonde data to the sum of three sine functions having 24-, 12-, and 8-hour periods and the 24-hour mean value. Figure 11 shows the result for Brisbane. The stars are the ionosonde wind medians, the solid line is the fit, the dashed lines are, in order of shortening dashed, the 24, 12, and 8-hour sinusoids. The 24-hour mean value was also included in the fit. The 24-hour mean of the data shown in Figure 11 is -1.1 *m/s*.

Figure 12 shows the amplitude of the three waves for a sequence of northern mid-latitude ionosonde stations surrounding the globe. The geographic locations of these stations are shown in Figure 13. The stations are centered at about 50 degrees north latitude, although there are large differences in latitudes. The amplitude of each component is strongly dependent on the latitude of the station; the farther the station is from the equator, the greater is the amplitude of the wave.

Figure 14 shows the relative phases of the three sine waves. The fit was made to data that were specified by UT. In this case, the phase is determined by the universal time when the sine function crosses zero, from negative (southward) to positive (northward). The downward progression of the phases in Figure 14 are a result of the increasing difference between UT and LT as a function of longitude. The three sinusoids maintain nearly the same phase relative to each other at all of these stations.

Similar plots of southern hemisphere stations are shown in Figure 15, 16, and 17. There are fewer stations from which to select a chain in the southern hemisphere, and the stations that are available cover a much greater range in latitude (Figure 16). This is reflected in the large range of amplitudes shown in Figure 15. The phase curves shown in Figure 17 show that constant relative phase is also maintained in the Southern Hemisphere. However, the phases at any given longitude differ by 180 degrees between Northern and Southern Hemispheres for all three waves.

Similar plots for the meridional chain of stations of Figure 10 are shown in Figures 18-20. The amplitude of the 24-hour component (Fig. 18) is seen to increase with latitude, as expected based on the general flow pattern away from the region of solar heating. There is a node in this component at the equator. The amplitudes of the 12 and 8 hour components have small equatorial maxima which seems to be at odds with the latitudinal variation of the amplitudes of these components for the longitudinal stations shown in Figures 12 and 15. Nodes appear in the 12 and 8 hour components at about -40 degrees and +40 degrees, respectively. The nodes are defined by the amplitude going to zero at a point where a phase reversal occurs. The stations that were chosen for the constant-latitude chains were apparently poleward of the latitudes of the nodes in the 12 and 8 hour components.

One result of the phase of the 12 and 8 hour components remaining constant across the equator can be seen in the comparison of a fit to the winds from the ionosonde at Yamagawa (Figure 21) with the fit to the Brisbane data shown in Figure 11. In the Southern Hemisphere, the shorter-period sinusoids are out of phase with the 24-hour components at night, resulting in an abatement of the equatorward wind. In the Northern Hemisphere they are in phase at night, giving one peak in the nighttime wind.

CONCLUSIONS

For most applications, the HWM87 model gives a representation of meridional wind that is in good agreement with average winds derived from *hmF2*, but with a minimum of computational effort. However, there are rapid variations that are derived with consistency from ionosonde data that depart significantly from the low-order harmonic representation of the HWM87 model.

Winds derived from IRI values of *hmF2* agree remarkably well with average winds derived from ionosonde measurements during the SUNDIAL-2 campaign. If these winds can be shown to be reliable in a general sense, this result will provide the opportunity of a global comparison for results of global circulation models.

A least-squares fit of median winds derived from ionosonde data demonstrates that a fairly simple representation of the winds in the *F*-region that is based on periodic base functions can give an accurate estimate of the average meridional wind in the thermosphere. More work is needed to extend this to a global description. It does, however, support the concept used by the HWM87 model, that an accurate estimate of the wind at *F*-region heights can be described using vector spherical harmonics.

Acknowledgments:

This work was supported by the National Science Foundation under grants ATM-87-15367, ATM-87-16036, ATM-87-13693, ATM-87-16036, and ATM-87-14461, and by the National Aeronautics and Space Administration under grants NAGW 922 and NAGW 996.

REFERENCES

Buonsanto M. J., Salah J. E., Miller K. L., Oliver W. L., Burnside R. G., and Richards P. G., 1989. Observations of neutral circulation at mid-latitudes during the Equinox Transition Study, *J. Geophys. Res.*, accepted for publication.

Burnside R. G., Behnke R. A., and Walker J. C. G., 1983. Meridional neutral winds in the thermosphere at Arecibo: simultaneous incoherent scatter and airglow observations, *J. Geophys. Res.*, **88**, 3181-3189.

Burnside R. G., Tepley C. A., and Wickwar V. B., 1987. The O^+-O collision cross-section: can it be inferred from aeronomical measurements?, *Ann. Geophysicae*, 5, 343-349.

Chandler M. O., Behnke R. A., Nagy A. F., Fontheim E. G., Richards P. G., and Torr D. G., 1983. Comparison of measured and calculated low-latitude ionospheric properties, *J. Geophys. Res.*, **88**, 9187-9196.

Crary D. J., and Forbes J. M., 1986. The dynamic ionosphere over Arecibo: a theoretical investigation, *J. Geophys. Res.*, **91**, 249-258.

Dudeney J. R., 1983. The accuracy of simple methods for determining the height of the maximum electron concentration of the *F2*-layer from scaled ionospheric characteristics, *J. Atmos. Terr. Phys.*, **45**, 629-640.

Hedin A. E., 1987. MSIS-86 thermospheric model, *J. Geophys. Res.*, **92**, 4649-4662.

Hedin A. E., Spencer N. W., and Kileen T. L., 1988. Empirical global model of upper thermosphere winds based on Atmosphere and Dynamics Explorer satellite data, *J. Geophys. Res.*, **93**, 9959-9978.

Miller K. L., Torr D. G., and Richards P. G., 1986. Meridional winds in the thermosphere derived from measurement of *F2* layer height, *J. Geophys. Res.*, **91**, 4531-4535.

Miller K. L., Salah J. E., and Torr D. G., 1987. The effect of electric fields on measurements of meridional neutral winds in the thermosphere, *Ann. Geophysicae* 5A, **6**, 337-342.

Miller K. L., and Torr D. G., 1987. A global study of meridional winds in the thermosphere, *Adv. Space Res.*, **7**, (10)299-(10)302.

Rawer K., Bilitza D., and Ramakrishnan S., 1978. Goals and status of the International Reference Ionosphere, *Rev. Geophys. Space Phys.*, **16**, 177-181.

Rawer K., and Ramanamurty Y. V., 1985. International Reference Ionosphere--Status 1985/1986, URSI/COSPAR Workshop Proceedings, Belgium, 28 October 1985, Wheaton and Co. Ltd. (U.K.).

Richards P. G., and Torr D. G., 1985. Seasonal, diurnal, and solar cycle variations of the limiting H^+ flux in the earth's topside ionosphere, *J. Geophys. Res.*, **90**, 5261-5268.

Rishbeth H., 1966. *F2*-layer rates at sunspot minimum, *J. Atmos. Terr. Phys.*, 28, 911-918.

Young E. R., Torr D. G., Richards P., and Nagy A. F., 1980. A computer simulation of the midlatitude plasmasphere and ionosphere, *Planet. Space Sci.*, **28**, 881-893.

FIGURE CAPTIONS

Figure 1. Modelled height of the *F2*-layer in the absence of neutral winds for six ionosonde stations at approximately the same longitude. Geographic locations of the stations are included in Figure 10. The median magnetic and solar indices for the SUNDIAL-2 period were used in the model.

Figure 2. Modelled ratio (α) of the change in layer height with respect to the change in the neutral meridional wind speed for the six stations considered in Figure 1.

Figure 3. *F2*-layer height at Tokyo at the time of the SUNDIAL-2 campaign. Short dashes show the balance height computed by the FLIP model. Longer dashes are average *hmF2* values for the IRI predictions for September and October, 1986. The solid line is the 15-day median of *hmF2* derived from ionosonde critical frequency measurements.

Figure 4. K_p values for the SUNDIAL-2 campaign.

Figure 5. Meridional neutral wind speed (*m/s*) along magnetic meridians from the HWM87 model. Input parameters are appropriate for 28 September 1986, at 0 UT.

Figure 6. Meridional neutral wind speed (*m/s*) at 0 UT, derived from IRI model calculations of *hmF2*. Positive winds are northward along the magnetic meridian. IRI model parameters for September and October, 1986, were interpolated to September 28.

Figure 7. Meridional neutral wind speed (*m/s*) at 0 UT derived from ionosonde critical frequencies. Wind speeds have been averaged over 15 days, from 21 September through 5 October 1986. Symbols mark the locations of ionosondes.

Figure 8. Neutral wind from the HWM87 model projected onto the magnetic meridian, showing the dependence of the wind speed on magnetic activity.

Figure 9. Meridional neutral wind speed (*m/s*) at a chain of ionosonde stations at approximately constant latitude. Positive winds are northward. Stars are ionosonde winds; solid line, IRI winds; and dashed line, HWM87 winds. Open and shaded circles mark local noon and midnight.

Figure 10. Same as Figure 9 for a meridional chain of stations.

Figure 11. Least-squares fit of three sinusoids and a 24-hour mean value to median wind values derived from ionosonde data from the Brisbane ionosonde (27.5 S, 152.9). The three sinusoids comprising the fit are shown by the dashed lines. The 24-hour mean value of these data is -1.1 *m/s*.

Figure 12. Amplitudes of the sine waves from least-squares fits to ionosonde winds from a chain of stations near 50 degrees north latitude.

Figure 13. Locations of ionosondes whose data are used for Figures 12 and 14.

Figure 14. Phases of the sine waves from least-squares fits to ionosonde winds from a chain of stations near 50 degrees north latitude. Phase is computed relative to 0 hours UT. Downward progression of phase is the result of the difference between Local Time and Universal Time.

Figure 15. Same as Figure 12 for stations in the Southern Hemisphere. The range of latitudes is much greater for the Southern Hemisphere chain of stations, resulting in a large range of amplitudes.

Figure 16. Locations of ionosondes whose data are used for Figures 15 and 17.

Figure 17. Same as Figure 14, for stations in the Southern Hemisphere. The phase of each curve differs from the phase of the corresponding curve in the Northern Hemisphere by about 180 degrees.

Figure 18. Same as Figure 12 for a meridional chain of stations.

Figure 19. Locations of ionosondes whose data are used for Figures 18 and 20.

Figure 20. Same as Figure 14 for a meridional chain of stations. Nodes are recognized in the curves by a zero in amplitude (Figure 18) accompanied by a phase reversal. Nodes can be seen in the 24-hour wave near the equator, in the 12-hour wave near 40°S, and in the 8-hour wave near 40°N.

Figure 21. Same as Figure 11 for data from the Yamagawa ionosonde (31.2°N, 130.6°E).

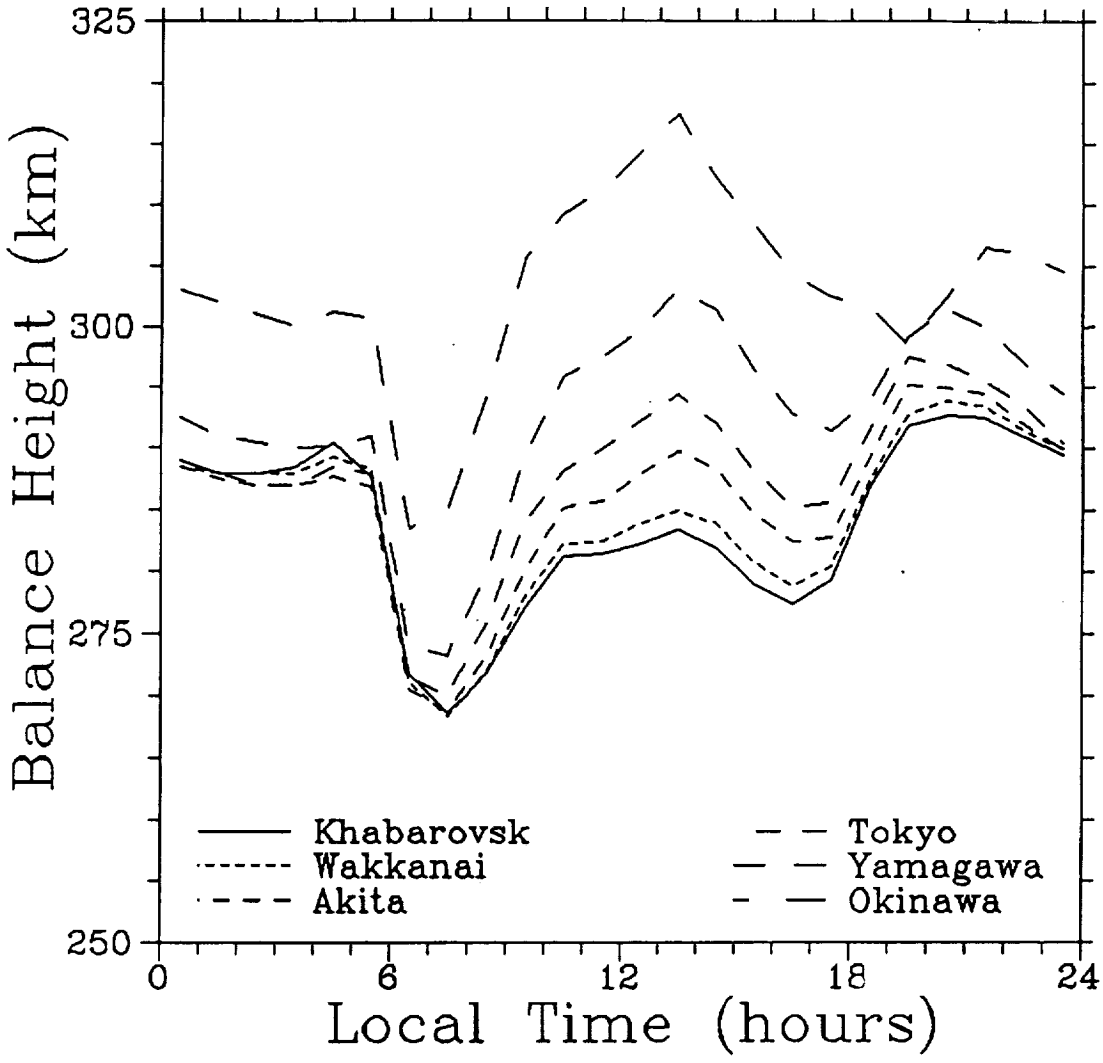

Fig. 1. Modelled height of the *F2*-layer in the absence of neutral winds for six ionosonde stations at approximately the same longitude. Geographic locations of the stations are included in Figure 10. The median magnetic and solar indices for the SUNDIAL-2 period were used in the model.

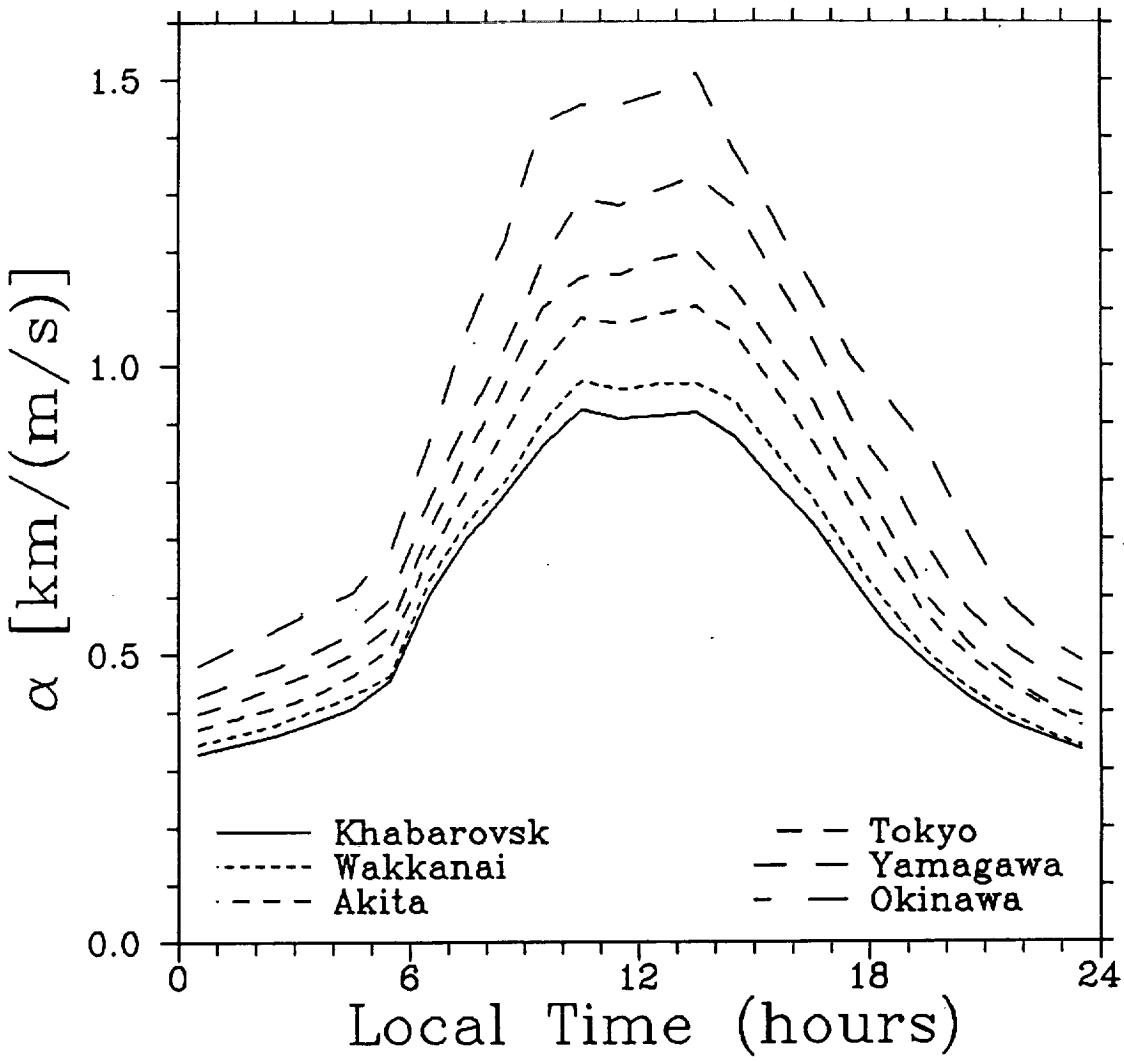

Fig. 2. Modelled ratio (α) of the change in layer height with respect to the change in the neutral meridional wind speed for the six stations considered in Figure 1.

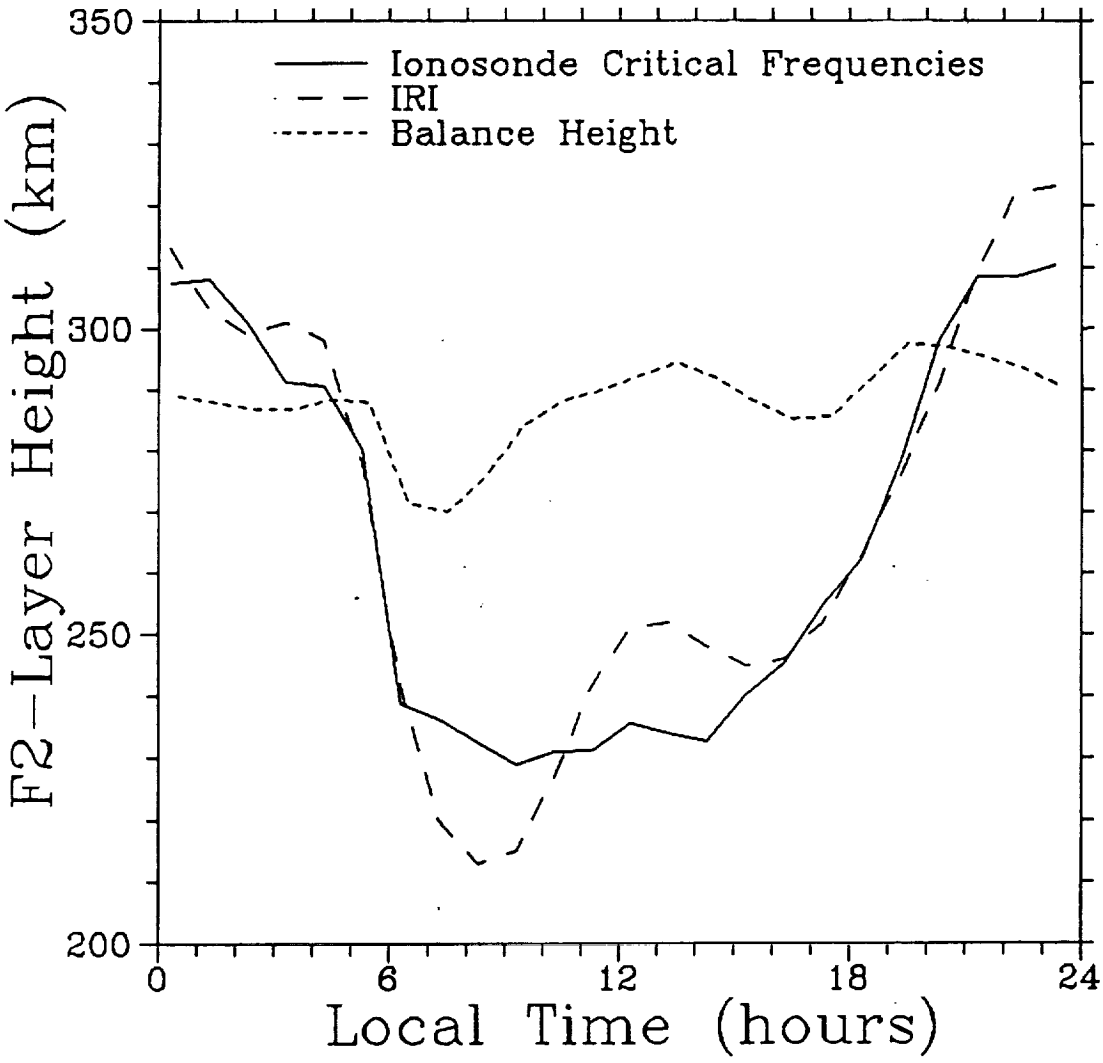

Fig. 3. *F2*-layer height at Tokyo at the time of the SUNDIAL-2 campaign. Short dashes show the balance height computed by the FLIP model. Longer dashes are average *hmF2* values for the IRI predictions for September and October, 1986. The solid line is the 15-day median of *hmF2* derived from ionosonde critical frequency measurements.

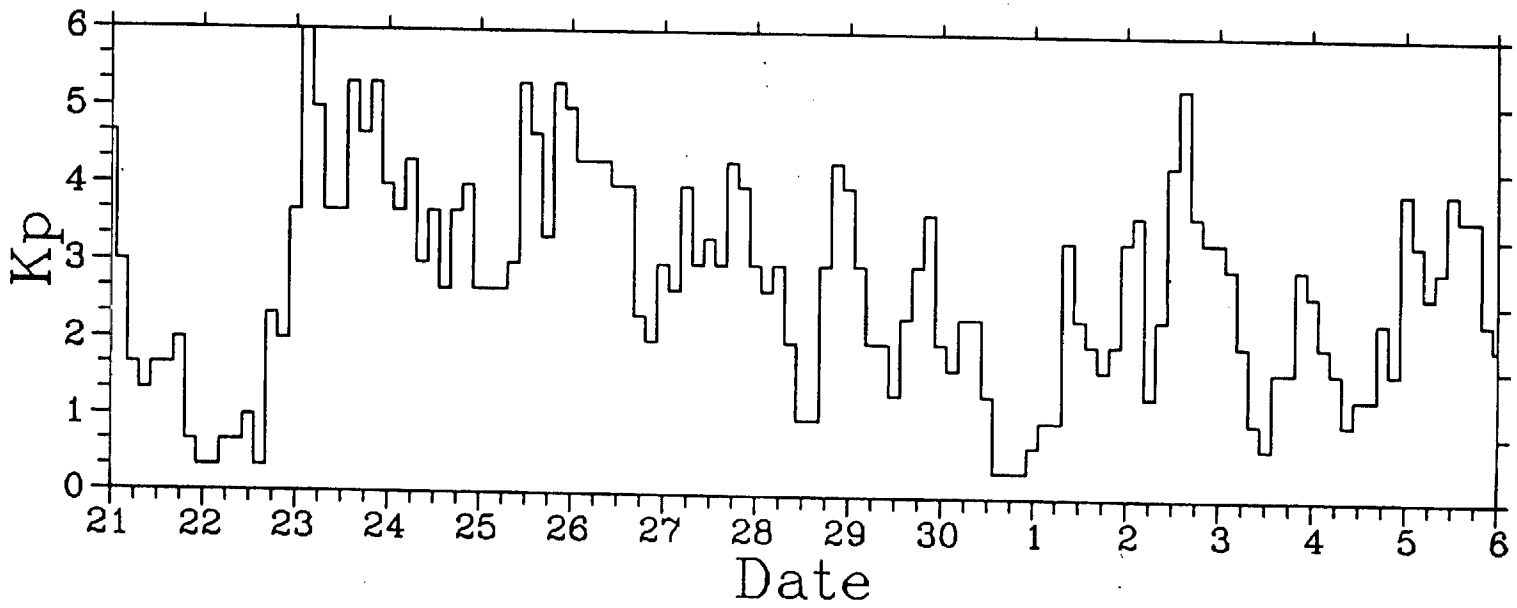

Fig. 4. K_p values for the SUNDIAL-2 campaign.

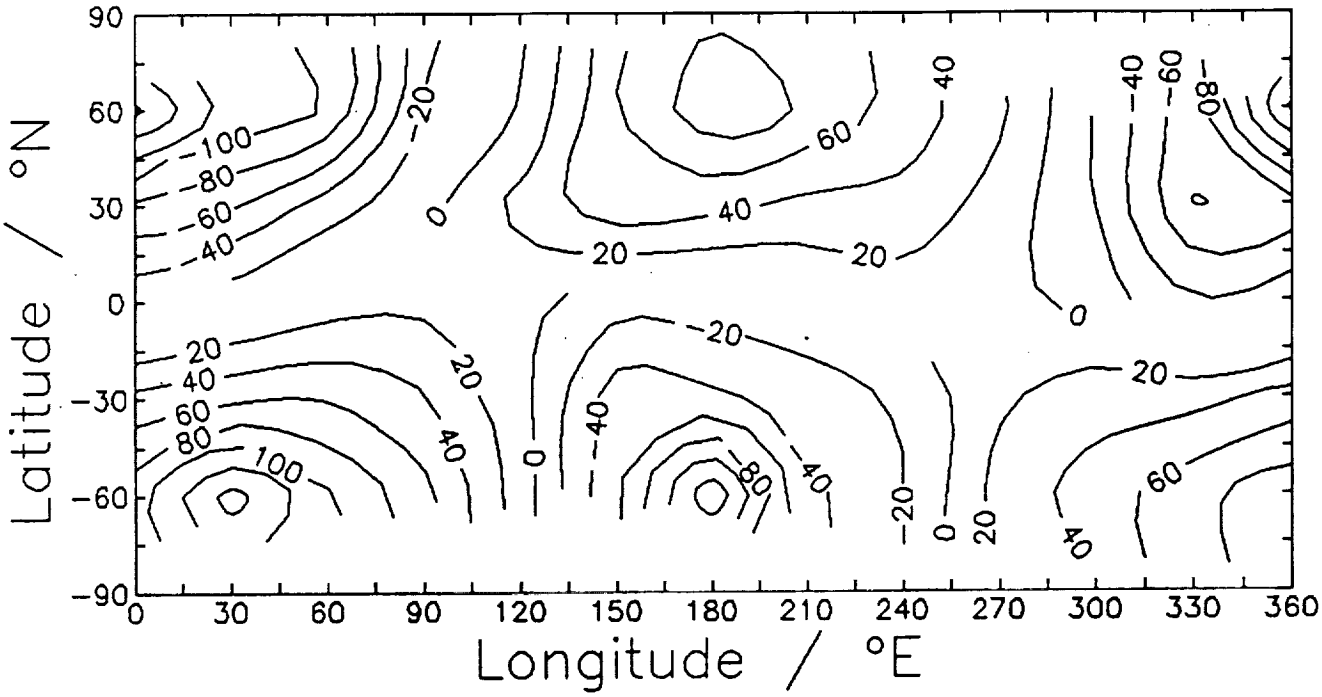

Fig. 5. Meridional neutral wind speed (*m/s*) along magnetic meridians from the HWM87 model. Input parameters are appropriate for 28 September 1986, at 0 UT.

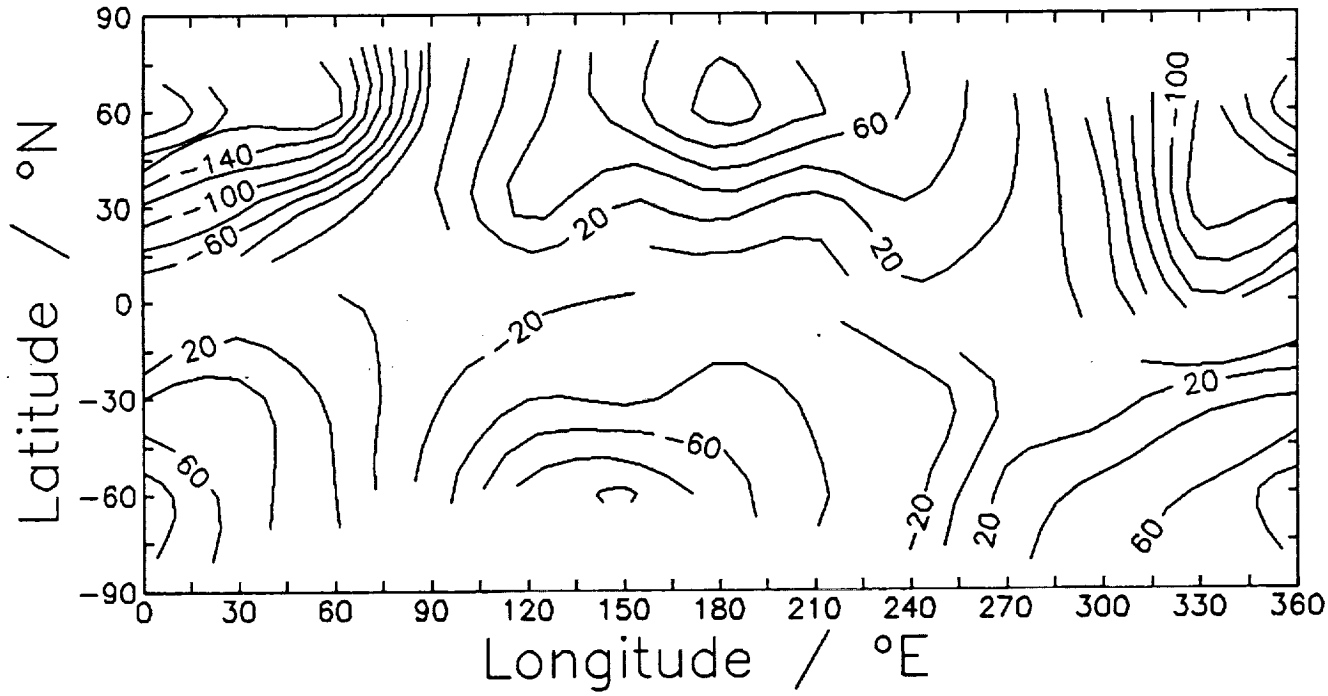

Fig. 6. Meridional neutral wind speed (*m/s*) at 0 UT, derived from IRI model calculations of *hmF2*. Positive winds are northward along the magnetic meridian. IRI model parameters for September and October, 1986, were interpolated to September 28.

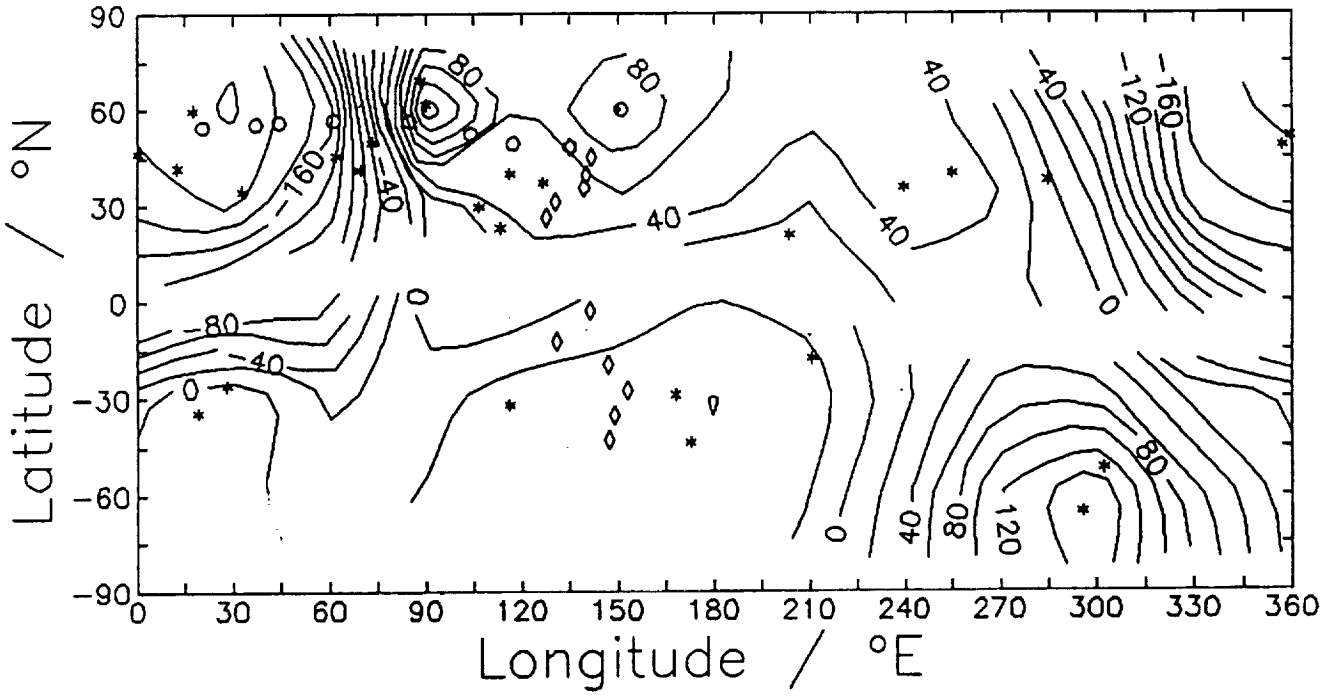

Fig. 7. Meridional neutral wind speed (*m/s*) at 0 UT derived from ionosonde critical frequencies. Wind speeds have been averaged over 15 days, from 21 September through 5 October 1986. Symbols mark the locations of ionosondes.

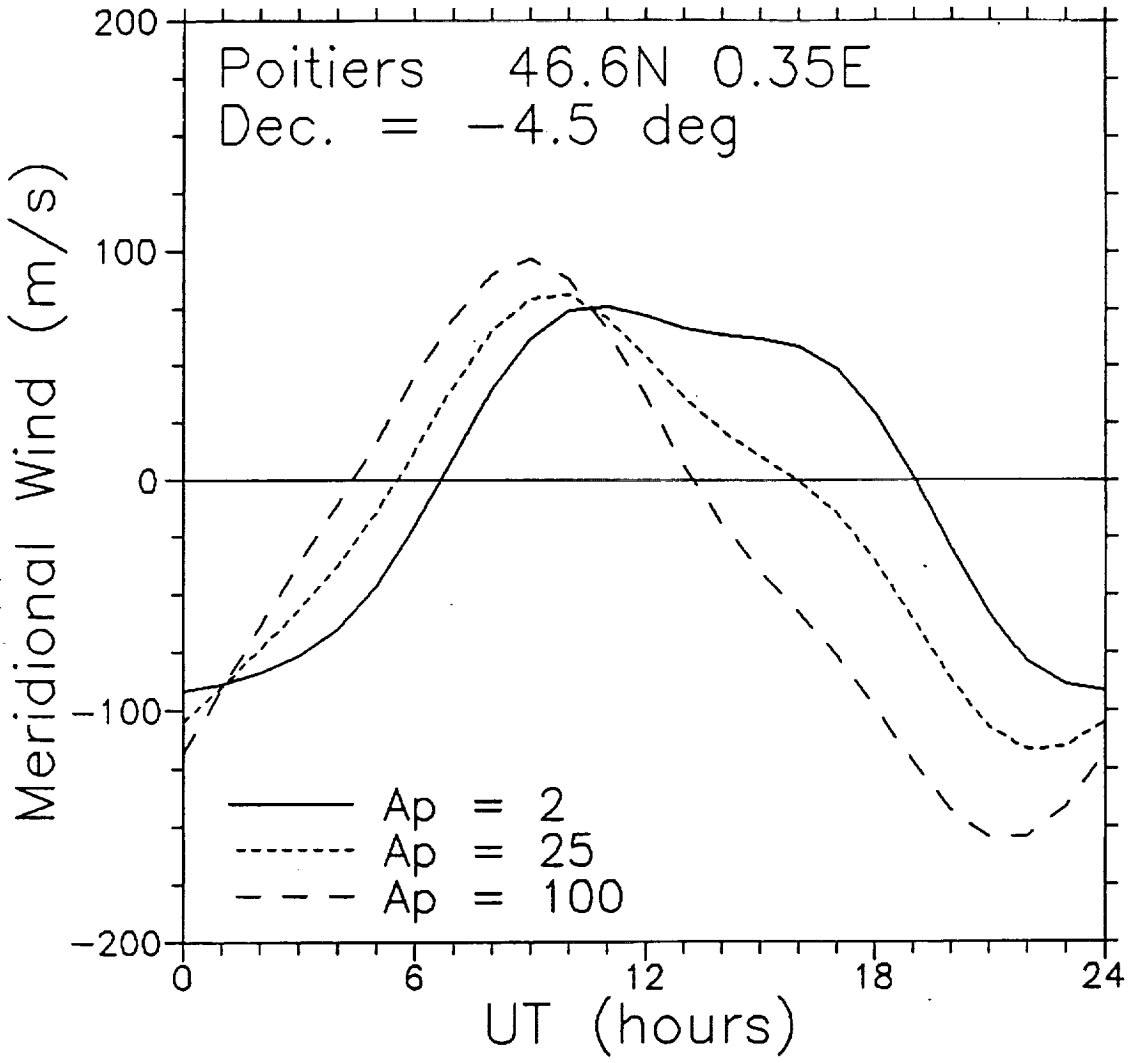

Fig. 8. Neutral wind from the HWM87 model projected onto the magnetic meridian, showing the dependence of the wind speed on magnetic activity.

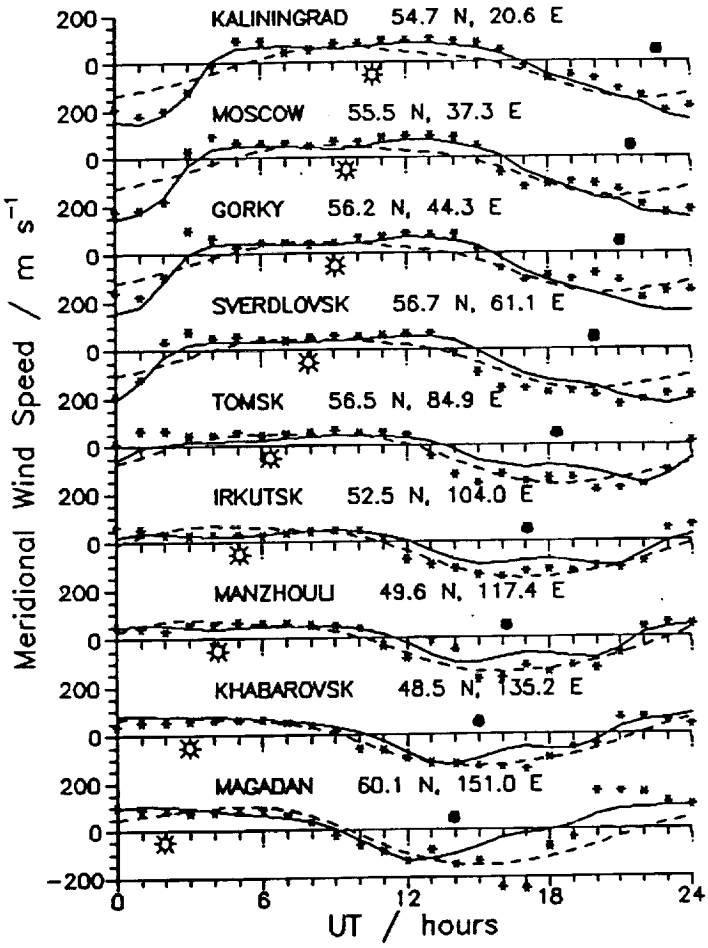

Fig. 9. Meridional neutral wind speed (*m/s*) at a chain of ionosonde stations at approximately constant latitude. Positive winds are northward. Stars are ionosonde winds; solid line, IRI winds; and dashed line, HWM87 winds. Open and shaded circles mark local noon and midnight.

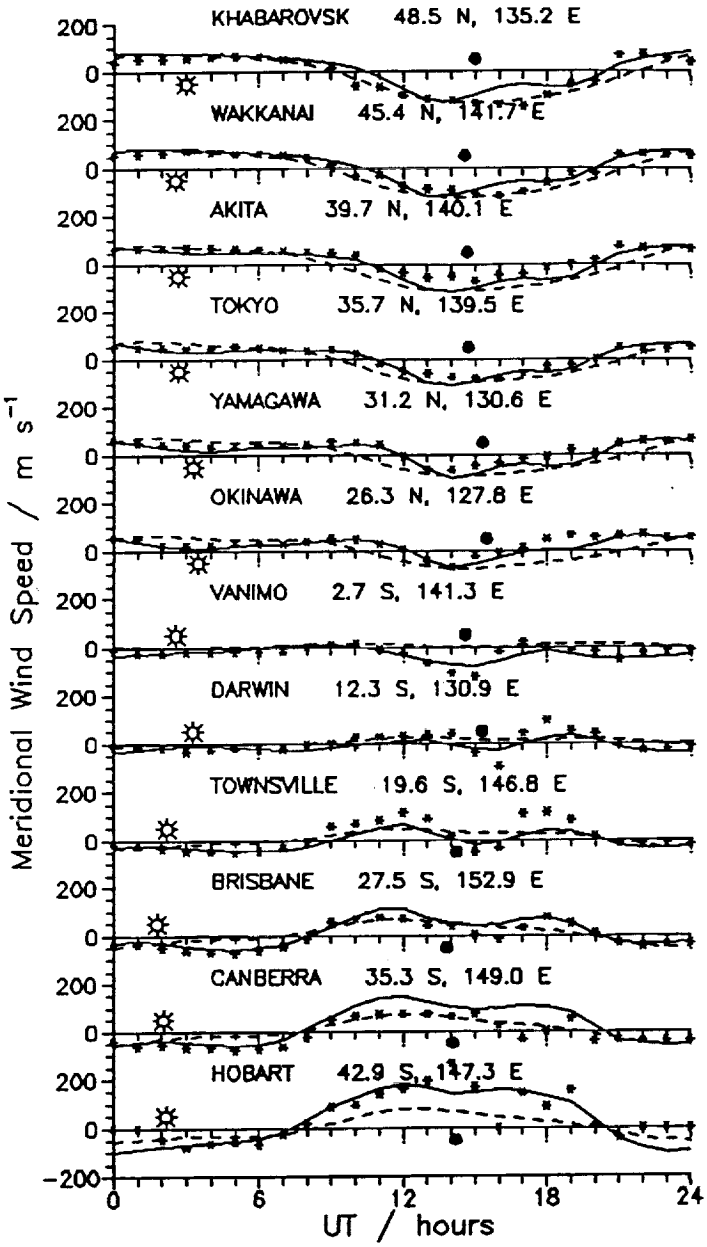

Fig. 10. Same as Figure 9 for a meridional chain of stations.

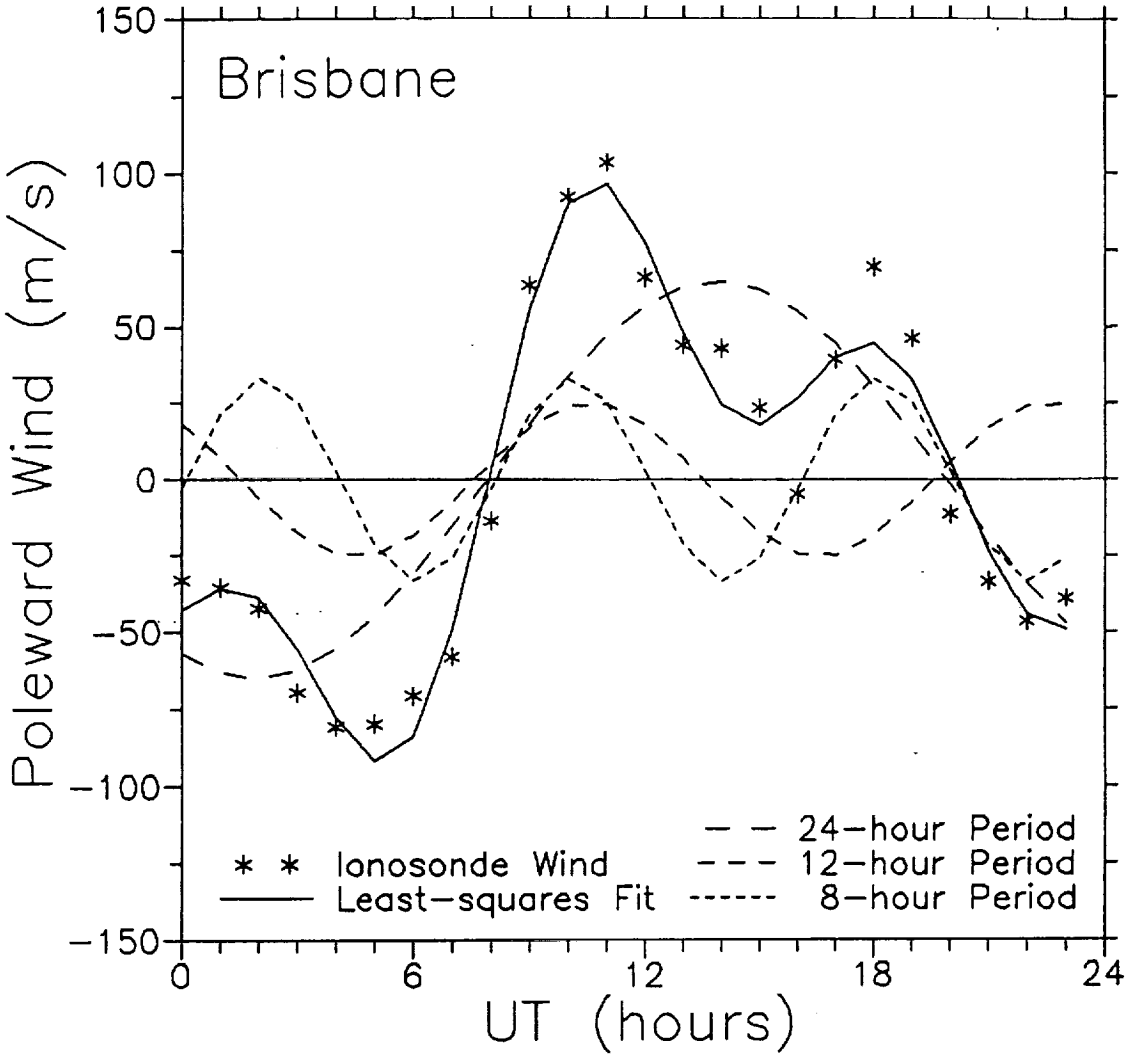

Fig. 11. Least-squares fit of three sinusoids and a 24-hour mean value to median wind values derived from ionosonde data from the Brisbane ionosonde (27.5 S, 152.9). The three sinusoids comprising the fit are shown by the dashed lines. The 24-hour mean value of these data is -1.1 *m/s*.

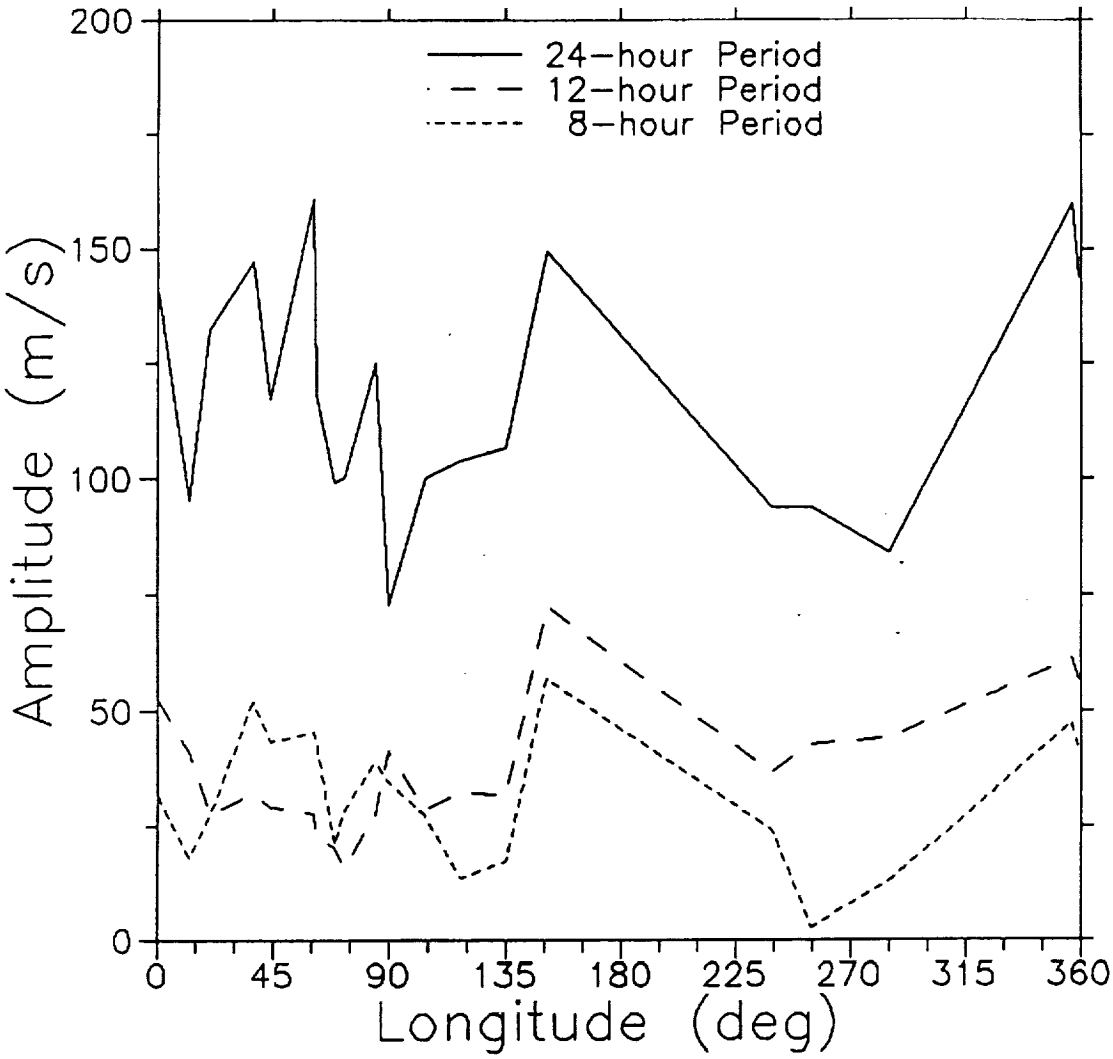

Fig. 12. Amplitudes of the sine waves from least-squares fits to ionosonde winds from a chain of stations near 50 degrees north latitude.

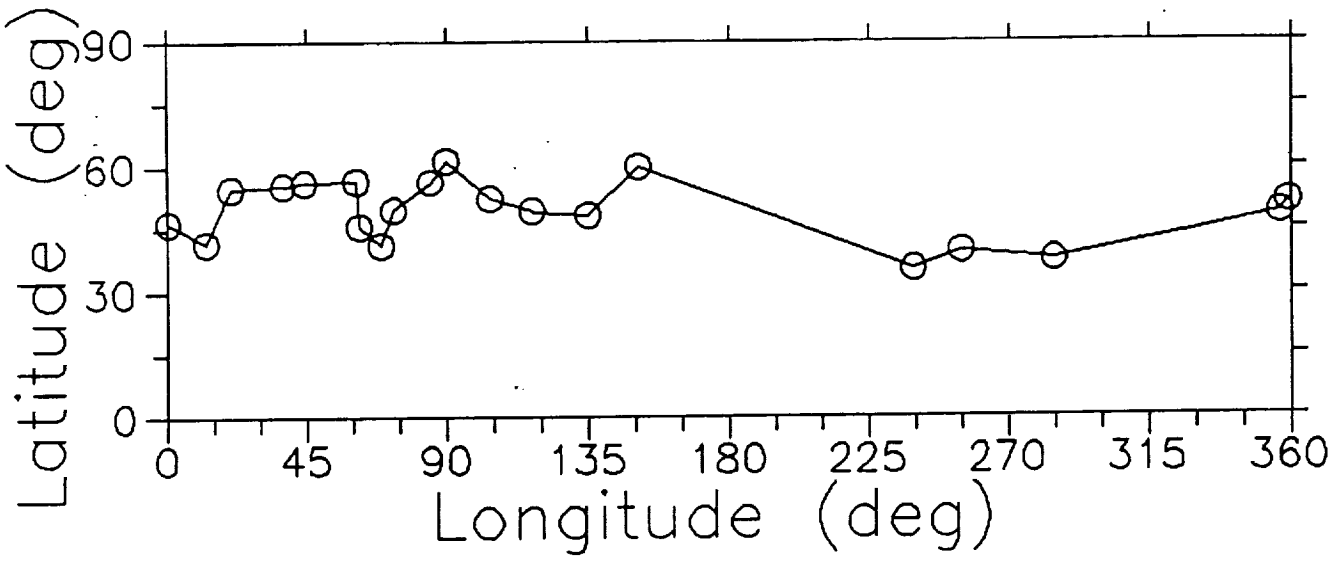

Fig. 13. Locations of ionosondes whose data are used for Figures 12 and 14.

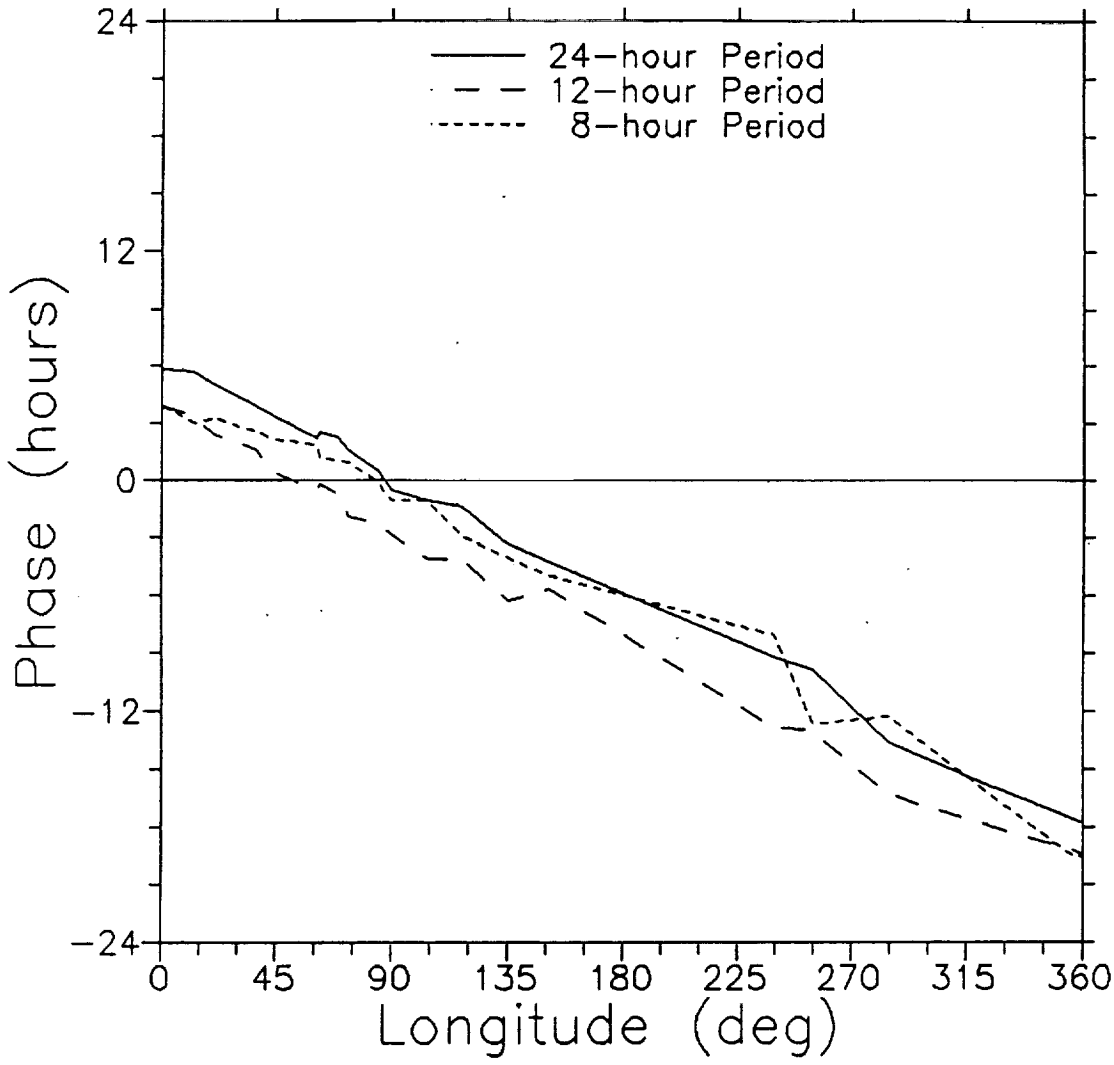

Fig. 14. Phases of the sine waves from least-squares fits to ionosonde winds from a chain of stations near 50 degrees north latitude. Phase is computed relative to 0 hours UT. Downward progression of phase is the result of the difference between Local Time and Universal Time.

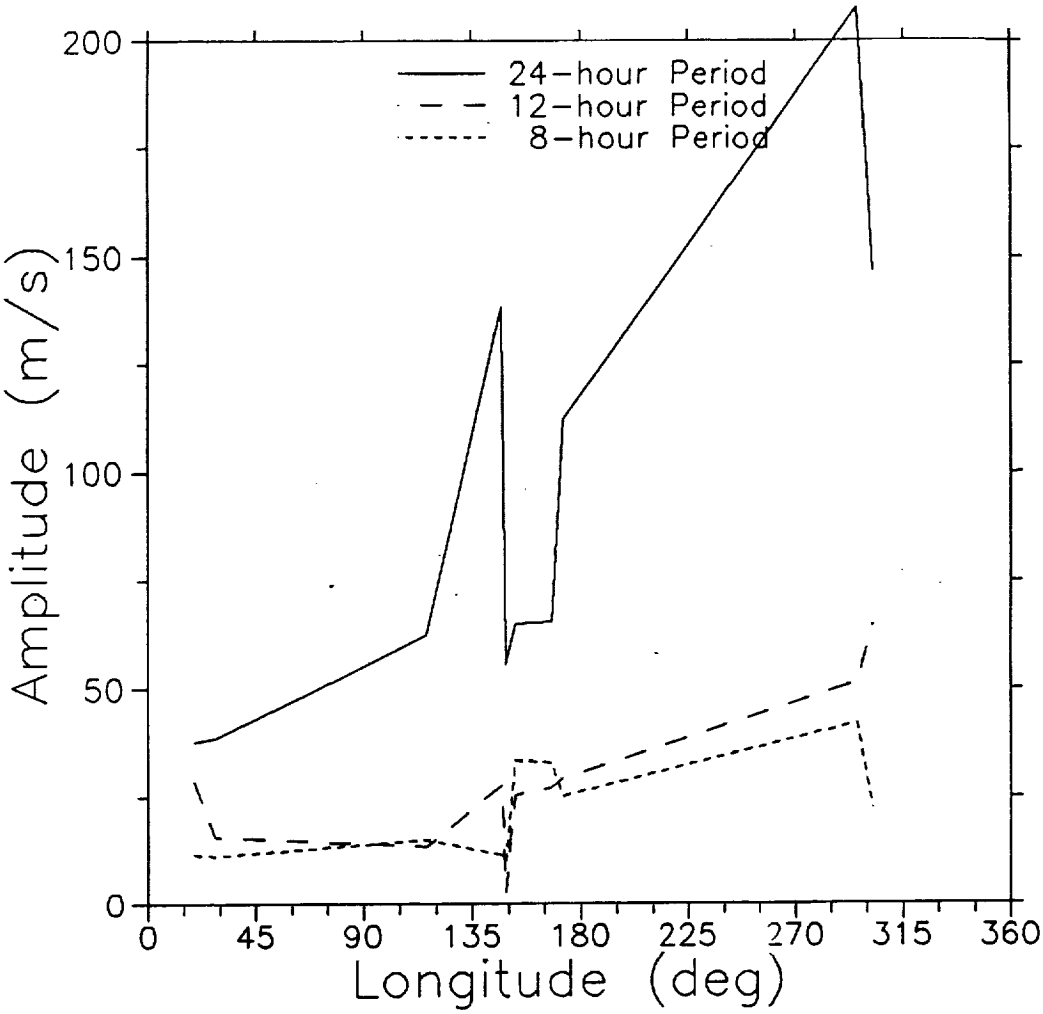

Fig. 15. Same as Figure 12 for stations in the Southern Hemisphere. The range of latitudes is much greater for the Southern Hemisphere chain of stations, resulting in a large range of amplitudes.

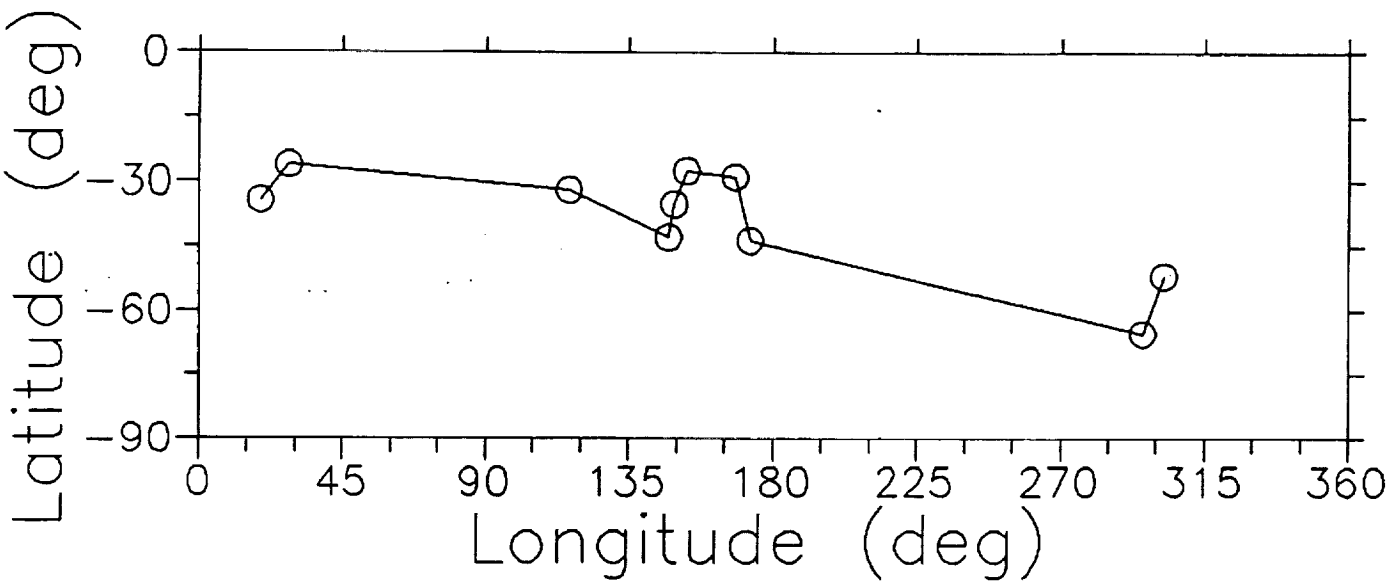

Fig. 16. Locations of ionosondes whose data are used for Figures 15 and 17.

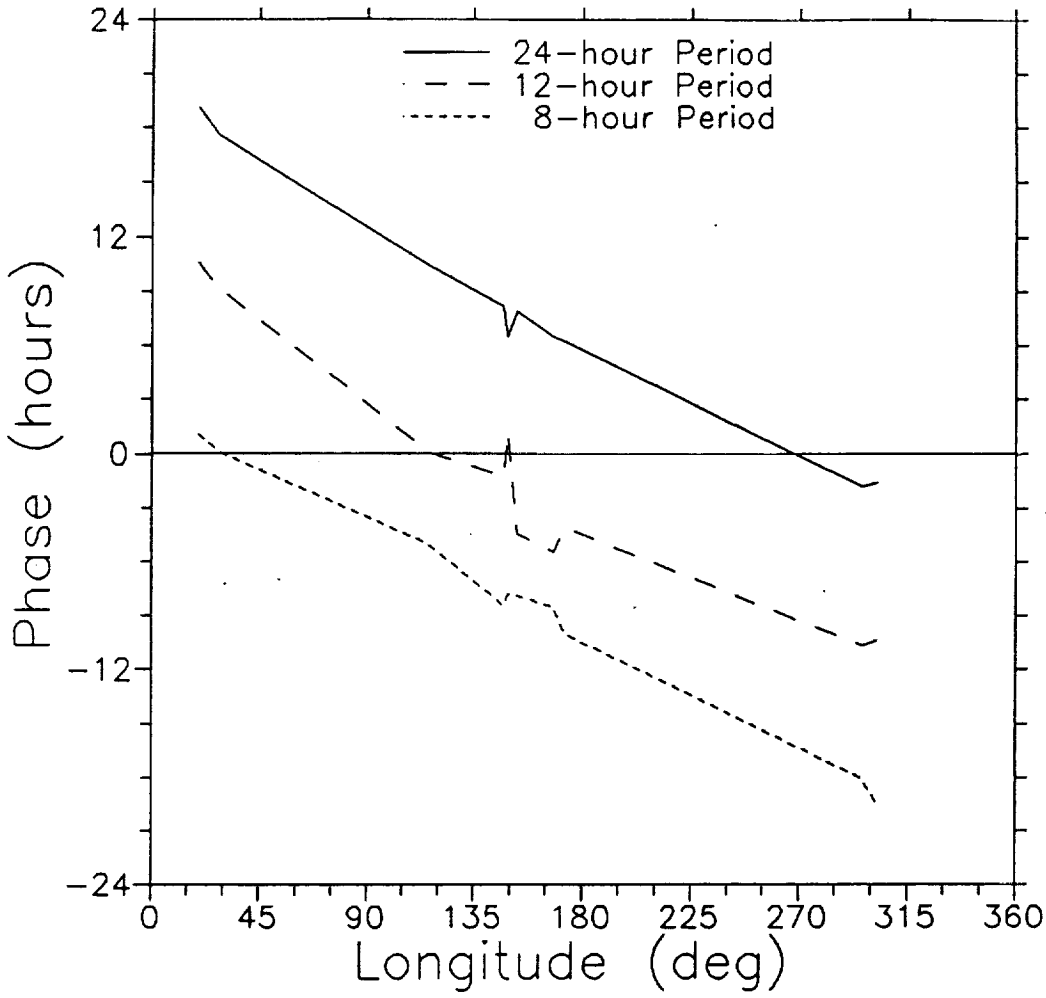

Fig. 17. Same as Figure 14, for stations in the Southern Hemisphere. The phase of each curve differs from the phase of the corresponding curve in the Northern Hemisphere by about 180 degrees.

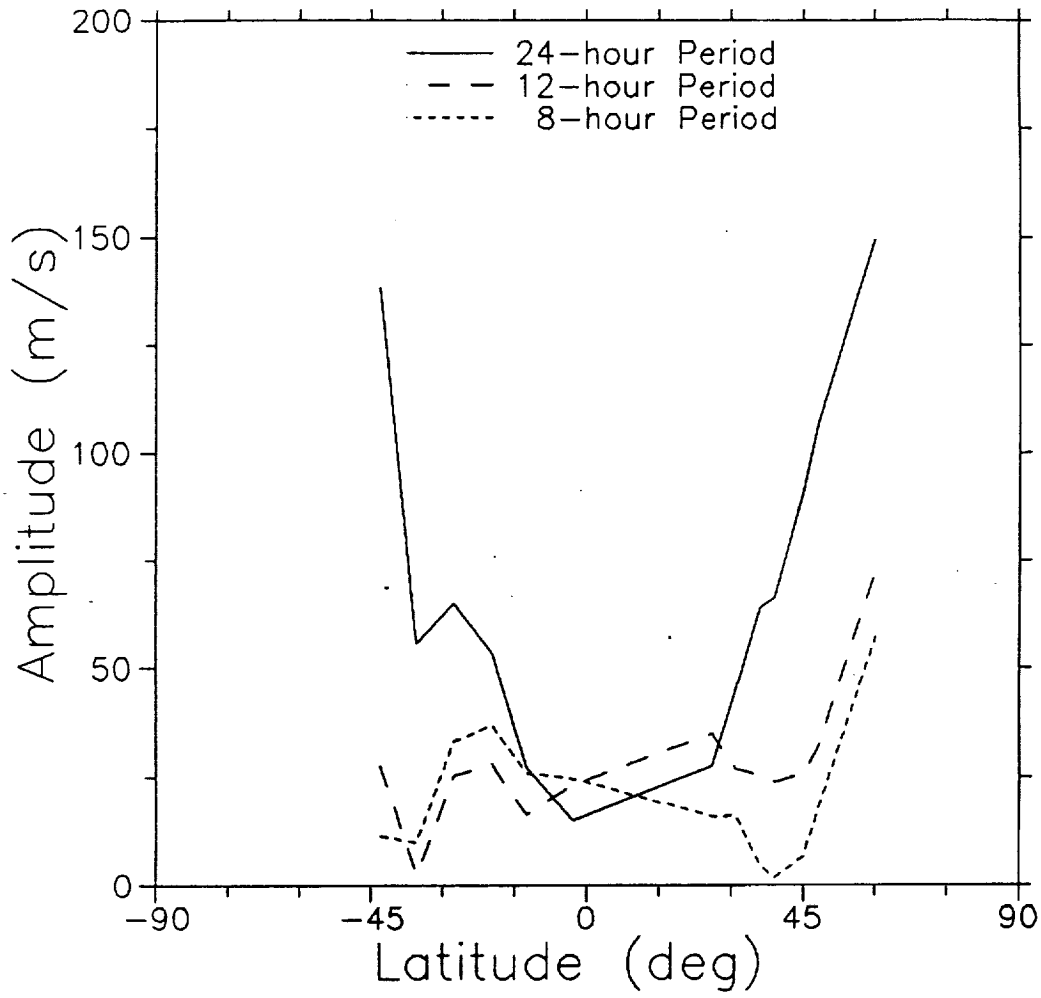

Fig. 18. Same as Figure 12 for a meridional chain of stations.

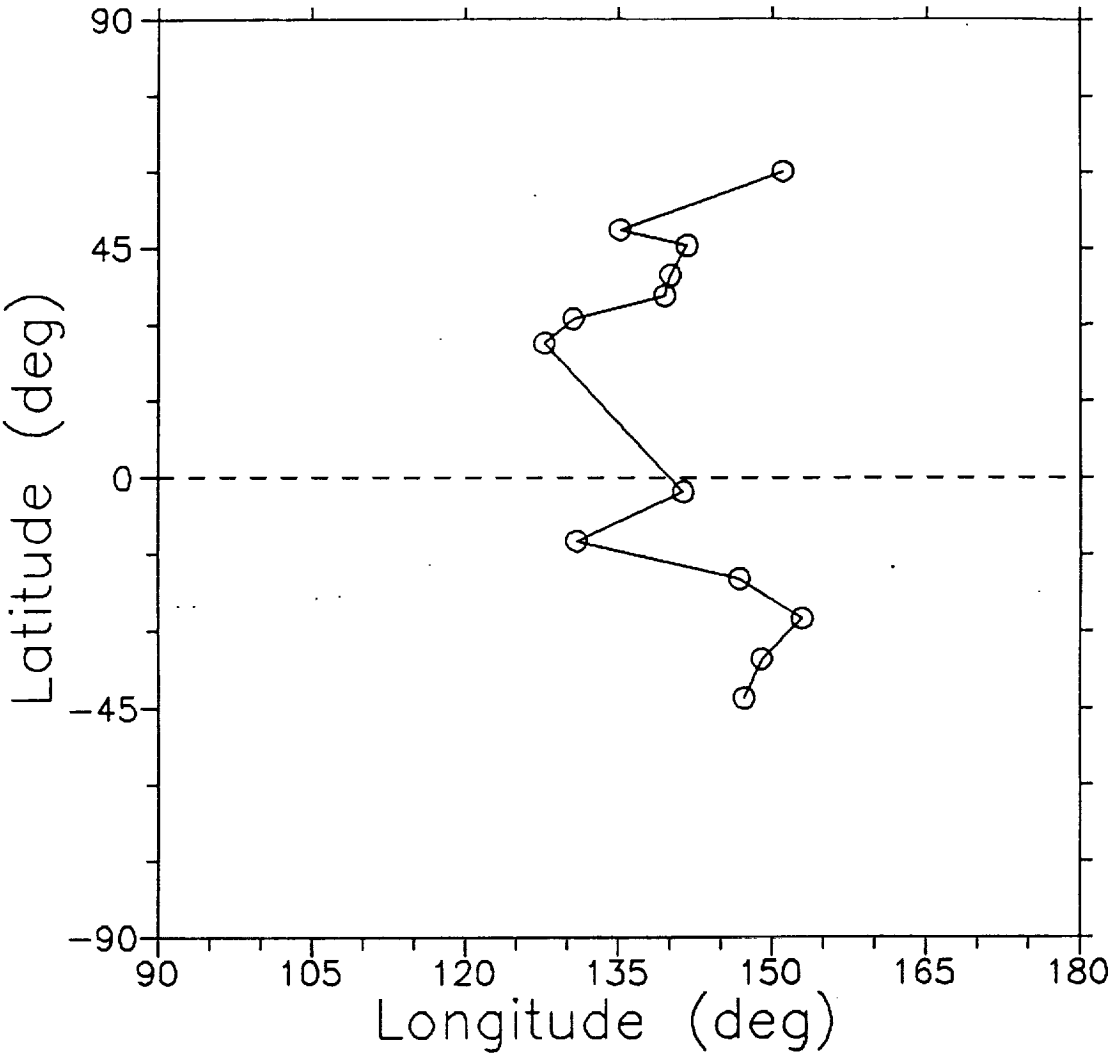

Fig. 19. Locations of ionosondes whose data are used for Figures 18 and 20.

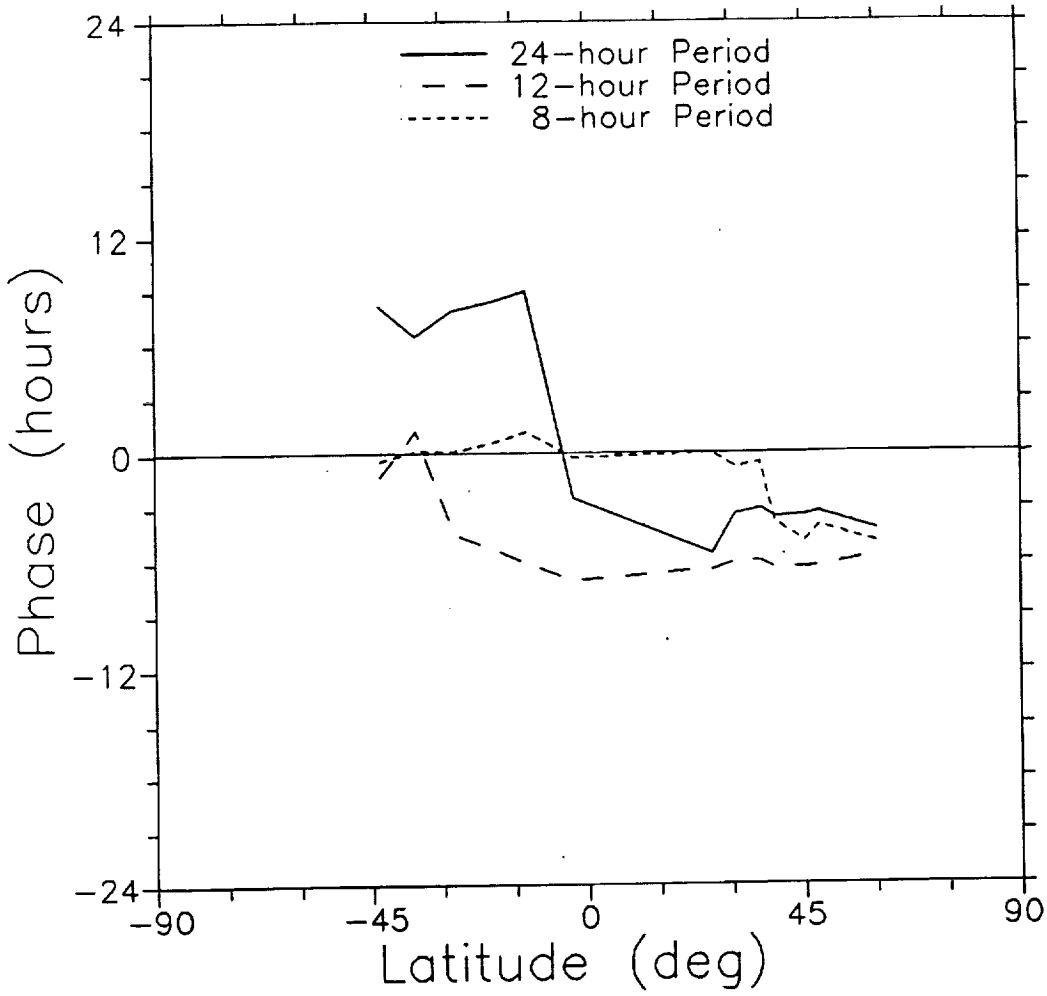

Fig. 20. Same as Figure 14 for a meridional chain of stations. Nodes are recognized in the curves by a zero in amplitude (Figure 18) accompanied by a phase reversal. Nodes can be seen in the 24-hour wave near the equator, in the 12-hour wave near 40°S, and in the 8-hour wave near 40°N.

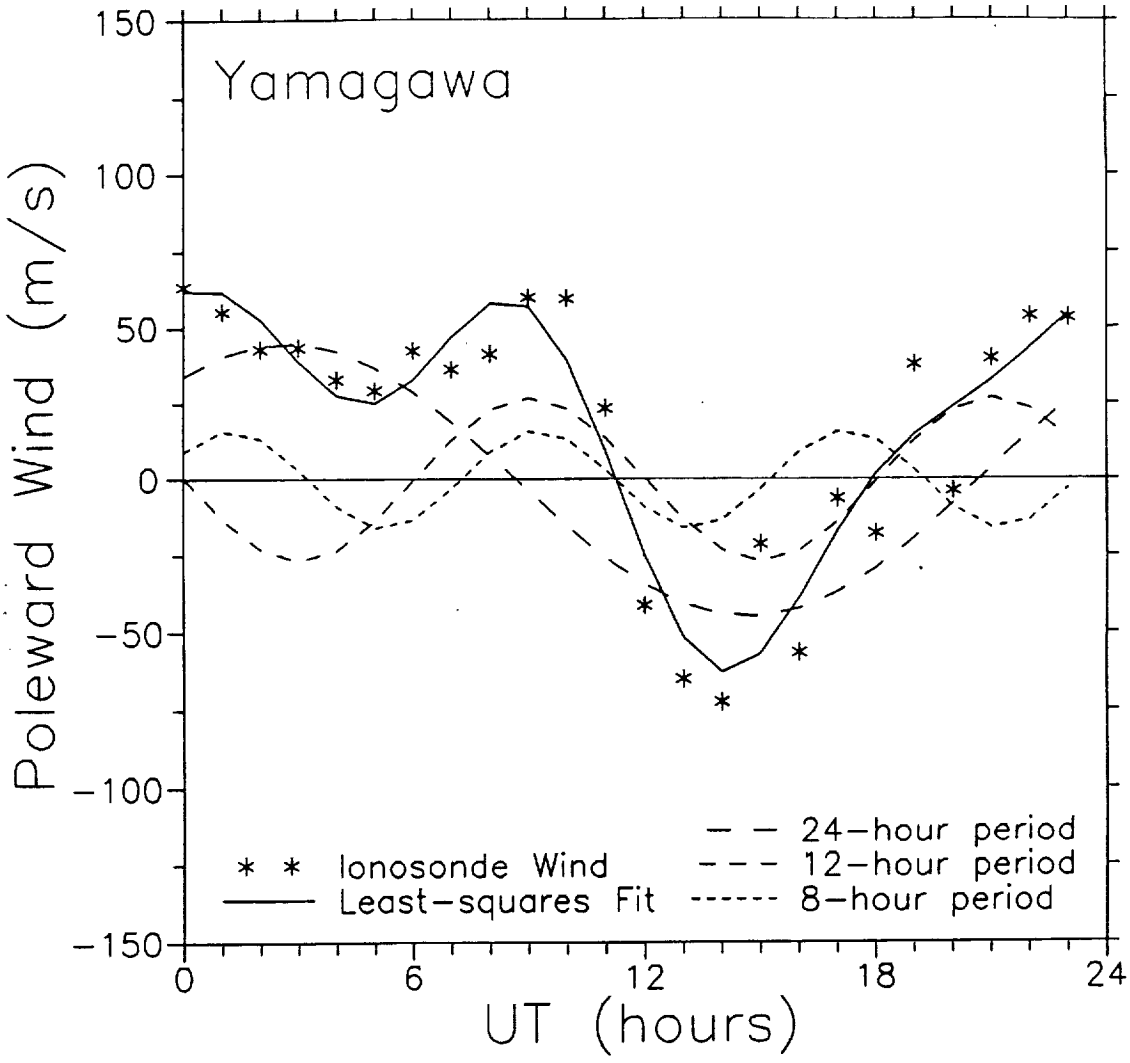

Fig. 21. Same as Figure 11 for data from the Yamagawa ionosonde (31.2°N, 130.6°E).